Dislocations in stripes and lattice Dirac fermions

Mesaroš, A.

Chapter 7

Coupled Nematic and Smectic Order in Underdoped Cuprates

Presence of various competing orders is one of the main characteristics of the high-T_c compounds ("cuprates"), especially in their pseudogap phase (see phase diagram in Fig. 1.7). The competition might be the key element for understanding of many unusual phenomena in cuprates, including the high value of T_c.

Among the different observed orderings, local lattice symmetry breaking seems to be ubiquitous. This invokes a quantum liquid crystal picture of the strongly correlated electron fluid in the cuprates [35, 100–102]. Accordingly, the local breaking of the square lattice symmetry (group C_{4v}) is quantified by smectic-like and nematic-like orders. The former breaks translational and orientational order, and was measured by neutron scattering in the form of well-known static stripes in LSCO and LBCO compounds [94–97], as well as in the fluctuating form in optimally doped YBCO [98]. The observation of the latter, nematic-type order is more recent in the cuprates (although known in other strongly correlated systems [248]). It was identified in YBCO [104,105] and possibly in HgBCO based compounds.

The superb cleavage properties of compounds like BSCCO and CNCOC have facilitated the Scanning Tunneling Microscope (STM) surface measurements of atomic resolution [99, 106]. These features have been interpreted in terms of the opposite limits of forming checkerboard patterns [249, 250], and $4a$ (a is lattice constant) wide periodic modulations [251, 252], which resemble stripes found in the bulk of cuprate crystals. The disordered stripe-like ordering and its influence on nodal quasiparticles and spin properties have already been investigated using

order parameter theory, in combination with numerical methods. One of the central issues has been discerning the role of external disorder, which at the same time can lead to shortening correlation lengths of ordering fields, as well as locally inducing order through pinning [250].

The coexistence of the two liquid crystalline-type orders in the STM data on BSCCO provides a possibility for a complete analysis of their interplay, and that is the goal of this Chapter. It turns out that the topological defects in the smectic (which are called "stripe dislocations") are a unique and important ingredient. Their presence (i) reveals the incommensurate nature of the stripes, (ii) provides for the main disorder mechanism leading to short stripe correlation lengths, and (iii) provides a unique signature in the nematic fluctuations through linear coupling terms.

We will start this Chapter with the description of experimental data (the Z-map), and how the order parameters are extracted. After a presentation of the nature of stripes and their disorder, we will continue with a Ginzburg-Landau theory description of coupled nematic and smectic fields. This will reveal some signatures of dislocations in the nematic fluctuations which are also observed in the data, corroborating the Landau field theory description. We will close the chapter with remarks on the connection to external disorder, and the emerging overall quantum liquid crystal picture.

7.1 General order parameters of the Z-map

It is well-known that in normal metals the differential tunneling conductance is proportional to the local density of states ρ:

$$\frac{\mathrm{d}I}{\mathrm{d}V} \equiv \bar{N}(\vec{r}, E) \sim \rho(\vec{r}, E). \tag{7.1}$$

In strongly correlated systems the situation is complicated by a space dependent prefactor, which suggests that local ratios of $\bar{N}$ should be used. It turns out that the asymmetry of tunneling conductance [253], called the Z-map,

$$Z(\vec{r}, E) = \frac{\bar{N}(\vec{r}, E)}{\bar{N}(\vec{r}, -E)}, \tag{7.2}$$

at low dopings becomes proportional to the doped hole density, and therefore represents a relevant charge-type order parameter at a given energy.

The Fourier analysis in Ref. [106] suggests that the Z-map data $Z(\vec{r})$ can be sensibly described as several modulated finite momentum waves given by a set of ordering wavevectors. This implies the model form $Z(\vec{r}) = \sum_a Re[\Phi_a e^{i\vec{Q}_a\vec{r}}]$, where a numbers the set of ordering wavevectors, and Φ_a are smooth complex fields. In this approach, the goal is to ascribe precise numerical quantities to the patterns seen clearly by eye in the real space Z-map. In that Reference, a

technique for extracting the slowly varying Φ_a order parameter fields is presented: the Fourier data of the Z-map around the wavevector $\vec{Q}_a$ is shifted to the origin, and transformed back to real space, after a cutoff is chosen to remove all other peaks in the data:

$$\bar{\Phi}_{\vec{Q}_a}(\vec{r}) = \sum_{\vec{k}} \tilde{Z}_a(\vec{Q}_a + \vec{k}) e^{i\vec{k}\cdot\vec{r}} e^{-k^2/2\Lambda}. \tag{7.3}$$

One finally gets $\Phi_a(\vec{r}) = \sum_{\vec{q}} \bar{\Phi}_{\vec{Q}_a}(\vec{q}) e^{i\vec{q}\cdot\vec{r}}$ as a smoothed field, with wavelengths smaller than $1/\Lambda$ suppressed. Similarly, from the data near $-\vec{Q}_a$ one gets $\Phi^*_a(\vec{r})$.

7.1.1 Symmetry properties

The C_4 group has four irreducible representations, given by $A_0(c_4) = 1$, $A_1(c_4) = i$, $A_{-1}(c_4) = -i$, $A_2(c_4) = -1$, where c_4 is the $\pi/2$ rotation group element that generates the group. Going to C_{4v} by adding the reflection across y axis σ_x couples the A_1 and A_{-1} representations into the two dimensional E_1, and duplicates A_0 and A_2, with $\sigma_x \to \pm 1$.

By definition, the observable Z-map does not change under (passive) symmetry transformations, i.e. $Z'(\vec{r}') = Z(\vec{r})$, where $\vec{r}' = R(g \in C_{4v})\vec{r} + \vec{t}$; R is the rotation matrix, and $\vec{t}$ a lattice vector. Because of the square symmetry of the Z-map, all order parameters will be associated with four Fourier wavevectors, i.e. $\vec{Q}_a \in \{\vec{Q}_x, \vec{Q}_y\}$ and $a = x, y$. From the chosen definition of $Z(\vec{r})$ we get the group representation D acting on the fields

$$\begin{pmatrix} \Phi'_a(\vec{r}') \\ \Phi^{*\prime}_a(\vec{r}') \end{pmatrix} = D(g) \begin{pmatrix} \Phi_a(\vec{r}) \\ \Phi^*_a(\vec{r}) \end{pmatrix}. \tag{7.4}$$

The result of this analysis are the irreducible components (σ_x acts trivially (as 1) on $Re[\Phi_\alpha]$):

$$\begin{aligned} Re[\Phi_x - \Phi_y] &\sim A_2 \\ Re[\Phi_x + \Phi_y] &\sim A_0 \\ Im[\Phi_x] \pm i Im[\Phi_y] &\sim A_{\pm 1} \\ \nabla_y \mp i \nabla_x &\sim A_{\pm 1}, \end{aligned}$$

where Φ_a represents the order parameter (OP) obtained from the information at the fixed wavevectors $\{\vec{Q}_a, -\vec{Q}_a\}$.

7.1.2 The nematic and smectic (stripe) orders

The Fourier transform of the Z-map reveals a small set of pronounced peaks, and these we use to define our order parameters.

We can identify the nematic OP, $O_n(\vec{r})$ by choosing $\vec{Q}$ to be the Bragg peak of the underlying CuO_2 lattice, i.e. $\vec{Q}_a = \frac{2\pi}{a}\vec{e}_a$., and choosing $O_n \sim A_2$. This

OP is responsible for the breaking of C_{4v} down to C_{2v}, and resembles a real Ising field. If we disregard any local information (coarse grain with an infinite radius, $\Lambda = 0$), the $O_n(\vec{r})$ becomes the constant

$$\langle O_n \rangle \sim \sum_{\vec{R}} Z(\vec{R}, O_x) - Z(\vec{R}, O_y), \tag{7.5}$$

which measures the difference of intensities on the two Oxygen sites (one along x and other along y axis with respect to central Copper atom) within the CuO_2 unit-cell, averaged on the whole lattice. Hence the name "intra-unit-cell" nematic OP.

We now proceed with identifying stripes with the OP at the wavevectors $\vec{S}_a \equiv \vec{Q}_a = \frac{3}{4}\frac{2\pi}{a}\vec{e}_a$, i.e. the "3/4" peaks which are also pronounced in the Z-map data. The two stripe orientations are described by the two OPs $\psi_x(\vec{r})$ and $\psi_y(\vec{r})$. We use the full complex fields $\psi_a \equiv \Phi_{\vec{S}_a}$ in the analysis, because of the non-trivial translational content, or in other words, the importance of phase fluctuations:

$$\psi_x(\mathbf{r}) = |\psi_x(\mathbf{r})| e^{i\varphi_x(\vec{r})} \tag{7.6}$$

$$\psi_y(\mathbf{r}) = |\psi_y(\mathbf{r})| e^{i\varphi_y(\vec{r})}, \tag{7.7}$$

The physical meaning of the *phase* φ_x, φ_y is that it is the phase of the charge density wave (CDW) with respect to the Copper site in the Z-map, i.e.

$$\psi_a(\vec{r}) \Rightarrow |\psi_a(\vec{r})| \cos(\vec{S}_a \cdot \vec{r} + \varphi_a(\vec{r})). \tag{7.8}$$

The OP fields $O_n(\vec{r})$ and $\psi_a(\vec{r})$ can now be characterized precisely using the dataset of the Z-map. In this thesis we only present characteristic results obtained from one dataset representing a $37a$ sized field of view (FOV), while actually the results of this analysis have been confirmed in a large collection of datasets of varying FOV sizes.

The first characterization of the OPs is that the nematic $O_n(\vec{r})$ develops an expectation value across the FOV as the Z-map energy reaches the pseudogap scale ($\approx$ 70meV); the smectic fields $\psi_a(\vec{r})$ stay disordered at all energies, in accordance with previous analyses. More precisely, for a general OP Ψ we use the correlation function

$$G_\Psi(\vec{r}) = \langle \Psi(\vec{r})\Psi(0) \rangle, \tag{7.9}$$

where the expectation value is the spatial average, $\langle \cdots \rangle \equiv 1/N \sum_{\vec{R}} \cdots$, with N the number of pixels with coordinates $\vec{R}$ in the Z-map. The Fourier transform of a typical polar angle averaged correlator G can be quite precisely fitted using just two terms: (i) the peak $\langle \Psi \rangle^2 \delta_{q,0}$, and (ii) a Lorentzian whose half width at half maximum is given by $(2\pi\xi)^{-1}$ where ξ is the spatial correlation length of the field $\Psi(\vec{r})$.

For the representative Z-maps at 102meV, we find that typically $\xi_S \approx 6a$ (a is the CuO_2 lattice constant), while the nematic develops an expectation

value [106]. The Gaussian smoothing of the fields done in the Fourier space of the Z-map corresponds to real space Gaussian smoothing with radius $\Gamma \sim 1/\Lambda \approx 4a$ of the size of cuprate stripe width, so that the stripe OP field is well defined. We see that the stripes are strongly disordered, with correlation lengths just above one stripe width.

7.1.3 Stripe dislocations

The understanding of the stripe disorder mechanism becomes much enriched by looking at the real space picture of the stripe phase fields φ_x, φ_y, Fig. 7.1(b,c).

We find that the stripe phase pictures are covered with vortex defects. Because the phase is periodic (i.e. it represents an angle on the unit circle), apart from smooth spatial variations it can host a *vortex*, a point defect in real space around which the phase winds a full circle ("from 0 to 2π"). If we follow any path in real space enclosing the dislocation, the phase will wind a full circle, a property robust to hypothetical local smooth changes in the value of the phase (as explained in the Introduction of this thesis).

The phase vortices here physically represents stripe dislocations, as illustrated in Fig. 7.1(d). Since our order parameter represents the modulation of the $3/4a$ wavevector, the smallest winding means that one of the three wave crests disappears at the core, within the $4a$ stripe width. We can demonstrate the appearance of stripe dislocations directly in the real space Z-map, by identifying the stripe wave crest (high intensity values) that abruptly ends at the defect core, Fig. 7.1(e).

The role of these topological defects is prominent, since we can quite precisely simulate the entire stripe phase FOV $\varphi_a(\vec{r})$ as just a linear superposition of single dislocation fields $\varphi^{(d)}(\vec{r})$, if assign the correct positions and winding numbers to all defects. The single stripe dislocation phase field $\varphi^{(d)}(\vec{r})$ is just given by the polar angle (θ):

$$\varphi^{(d)}(\vec{r}) \equiv \pm n\theta, \tag{7.10}$$

where $\pm$ chooses the winding $\pm n2\pi$. We always find the simplest dislocations in the data, with windings $\pm 2\pi$. Concerning the stripe amplitude, it is suppressed to zero near the defects, as is necessary because of the phase singularity. Furthermore, it seems the amplitudes of both x and y directed stripes are suppressed near any particular defect, as exemplified in the dataset of Fig. 7.2. We will comment on this in the discussion Section.

At this point we can assess the physical significance of the ubiquitous defects. The fact that the stripe CDW has such a strongly disordered phase, where all values between 0 and 2π appear throughout the FOV, suggests that these cuprates host incommensurate stripes. In the case of commensuration, domains of constant phase φ_a would prevail. the value of this constant would determine if the stripes are site centered (φ_a even multiple of $\pi/2$), bond centered (φ_a odd multiple of $\pi/2$), etc. We remark that, beside the fact that the phases are dis-

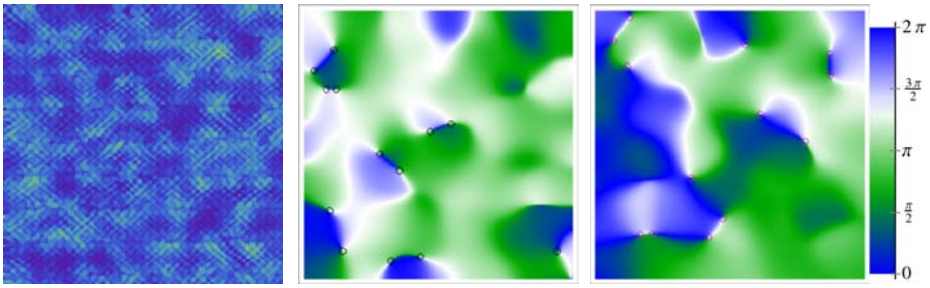

(a) Real space Z-map at 102meV, used throughout

(b) Real space map of φ_x, the phase of ψ_x, with vortices marked by black circles

(c) Real space map of φ_y, the phase of ψ_y, with vortices marked by purple circles

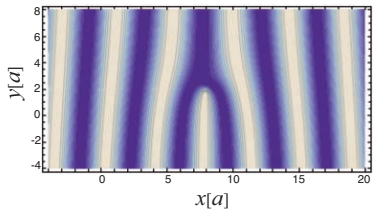

(d) Stripe dislocation in a $3/4a$ density wave, with phase winding $+2\pi$

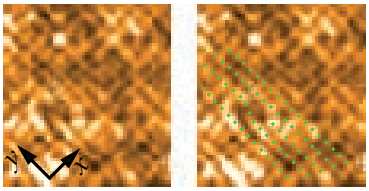

(e) Actual stripe dislocation in ψ_x identified in the real space Z-map

Figure 7.1: Stripes and their defects in the Z-map

tributed continuously and evenly between 0 and 2π, we do find that at the places where the stripe amplitude is maximal, the local phase value shows prevalence of bond-centeredness.

The fact that the stripes are incommensurate with the lattice implies that the phase of the CDW is a soft degree of freedom, i.e. it has gapless spectrum; this is in contrast to the case of commensurate CDWs, where finite energy is needed to locally change the phase. This further implies that the phase is an important degree of freedom to be included in the (therefore Ginzburg-) Landau theory of the smectic.

Just as in the case of vortices (see Introduction), the energy of an isolated stripe dislocation diverges with the system size. The fact that numerous dislocations are distributed throughout the system suggests that there is an additional degree of freedom that couples to the smectic and lower the energy of the defects. We therefore find *a priori* justification in considering a coupled smectic and nematic OPs. This situation is analogous to the case of classical liquid crystals described by de Gennes: the nematic fluctuations lower the energy of smectic defects, thereby melting the quasi-long-range smectic-A order into the nematic crystal. It must be noted that the present cuprate "smectic" and "nematic" OPs should be treated more carefully. As we will discuss at the end of this Chap-

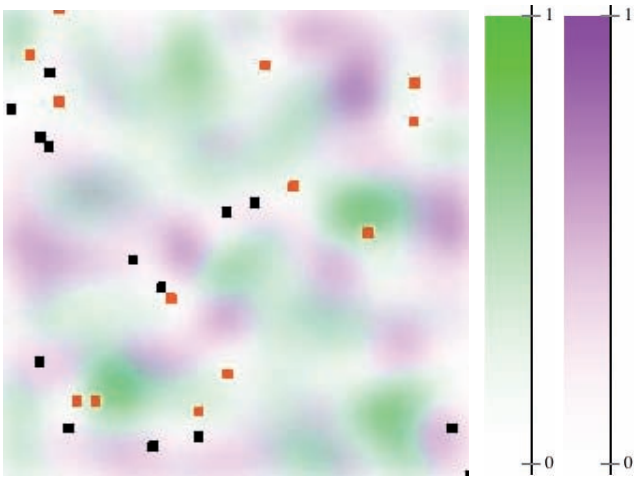

Figure 7.2: Stripe amplitudes, with defect positions superimposed: $|\psi_x|^2$ (green, and defects are black points), and $|\psi_y|^2$ (purple, defects are red dots)

ter, the relation between these two OPs does not completely correspond to the expectations from classical liquid crystals. Nevertheless, we now construct their GL theory, and show that such a description is corroborated by the data.

7.2 GL theory for the interplay of nematic and smectic

We start by considering the GL free energy for the smectic modulations. The general rules of Landau OP theory (see Introduction) is to form a functional that respects the symmetries of the system, which in our case are the crystal translations, and the C_{4v} square lattice point group. Actually, we consider terms allowed by an orthorombic crystal symmetry (C_{2v}), because according to the experimental data the square symmetry of the lattice is broken by the long range nematic order $\langle O_n \rangle \neq 0$. The stripe free energy becomes:

$$F_S[\psi_1, \psi_2] = \int \mathrm{d}^2\vec{r} \sum_{s=1,2} \Big[a_{x,s} |\nabla_x \psi_s|^2 + a_{y,s} |\nabla_y \psi_s|^2 + m_s |\psi_s|^2 \Big], \qquad (7.11)$$

written for both stripe modulations, where we replaced the stripe labels ψ_x, ψ_y by ψ_1, ψ_2, respectively, for the purpose of easier distinguishing from labels related to the derivatives ∇_x, ∇_y. We leave out terms beyond quadratic in stripe fields, as these are not involved in the subsequently proposed coupling to the nematic. We note that, in the context of Landau theory, treatment of the full Euclid group is nontrivial because it is infinite. Then the translational rule $\psi'_a(\vec{r}') = e^{-i\vec{S}_a \cdot \vec{t}} \psi_a(\vec{r})$

imposes the constraint of having an equal number of ψ_a and ψ_a^* in any term, modulo the allowed presence of multiples of four ψ_a, or four ψ_α^* factors (due to $4\vec{S}_a \equiv \vec{Q}_a^{\text{Bragg}}$). The treatment to higher order is necessary for numerical simulations, and such GL theories have been considered already [250, 251].

The relevant nematic degree of freedom in the C_{2v} phase, which is relevant for our analysis of the 102meV Z-map, is the fluctuation introduced as

$$O_n(\vec{r}) = \langle O_n \rangle + \delta O_n(\vec{r}). \tag{7.12}$$

A heuristic way of introducing a coupling between nematic and smectic electronic orders is to consider that a nematic fluctuation, depending on its sign, induces a local stretching or a local compression of the smectic modulation. We focus first on this coupling effect because it involves the phase of smectic. To implement it, we let the nematic fluctuation locally shift the smectic wavevectors:

$$\vec{S}_s \to \vec{S}_s + \vec{c}\,\delta O_n(\vec{r}). \tag{7.13}$$

The vector $\vec{c}$ is a phenomenological coupling constant. On the level of smectic modulations $\psi_s(\vec{r})$, the coupling of Equation (7.13) takes the form of a covariant derivative, i.e. the minimal coupling:

$$\nabla_i \psi_s(\vec{r}) \to (\nabla_i + i c_i \delta O_n(\vec{r}))\,\psi_s(\vec{r}). \tag{7.14}$$

Next we consider explicitly the coupling of nematic to the amplitude of the smectic. Based on crystal symmetries, a term linear in the nematic is allowed, taking the form:

$$\beta_s \delta O_n(\vec{r}) |\psi_s(\vec{r})|^2, \tag{7.15}$$

with β_s two phenomenological constants. It is the term of lowest possible order in amplitude of both fields, and describes a local enhancement of smectic amplitude fluctuation caused by the nematic fluctuation.

The substitution of the postulated minimal coupling of Equation (7.14), and the amplitude coupling of Equation (7.15), into the smectic free energy $F_S[\psi_1, \psi_2]$ from Equation (7.11), leads to the final form of the free energy describing the coupled nematic and smectic orders:

$$\begin{aligned} F_{GL}[\delta O_n, \psi_1, \psi_2] &= F_n[\delta O_n] + \\ &\int \mathrm{d}^2\vec{r} \sum_{s=1,2} \Big[\sum_{i=x,y} a_{i,s} |(\nabla_i + i c_i \delta O_n)\psi_s|^2 + m_s |\psi_s|^2 + \beta_s \delta O_n |\psi_s|^2 \Big] = \\ &= F_n[\delta O_n] + F_S[\psi_1, \psi_2] + \\ &+ \int \mathrm{d}^2\vec{r} \sum_{s=1,2} \sum_{i=x,y} \left[\alpha_{i,s} \delta O_n |\psi_s|^2 \nabla_i \varphi_s + \beta_s \delta O_n |\psi_s|^2 + \gamma_s \delta O_n^2 |\psi_s|^2 \right]. \end{aligned} \tag{7.16}$$

The form of the nematic free energy $F_n[\delta O_n]$ is delayed to Section 7.4. In the second line we have isolated the coupling terms, and introduced compact labels

for the coupling constants $\alpha_{i,s} = \sum_{i=x,y} a_{i,s} c_i$ and $\gamma_{i,s} = \sum_{i=x,y} a_{i,s} c_i^2$. The free energy $F_{GL}[\delta O_n, \psi_1, \psi_2]$ actually contains all the lowest order (up to quadratic in each field) coupling terms which are allowed by the reduced crystal symmetries (C_{2v}). Equation (7.16) is therefore the correct form of $F_{GL}[\delta O_n, \psi_1, \psi_2]$, which we would have obtained directly by symmetry considerations, bypassing the heuristic introduction of minimal coupling of Equation (7.14). The phenomenological coupling constants $\alpha_{i,s}$, β_s and γ_s are therefore independent. As we discuss in Section 7.4, the most important effects of the smectic dislocations come from the direct linear coupling of the nematic fluctuation and the smectic phase, described by the coupling constants $\alpha_{i,s}$.

7.3 Phenomenological GL parameters from cross-correlations

We can estimate the relative significance of the GL phenomenological couplings by evaluating the cross-correlation of corresponding fields. If these correlations between the two OP fields is significant, we can use it as a further proof of their coupling.

The coarse-grained OP field values inside the experimental field-of-view covered by the Z-map are represented by a discrete dataset. There are in total N data points, or pixels. The correlation coefficient of two datasets $\phi_{\vec{r}}$ and $\chi_{\vec{r}}$, where $\vec{r}$ is the datapoint coordinate, is:

$$C = \frac{\langle \phi_{\vec{r}} \chi_{\vec{r}} \rangle}{\sqrt{\langle \phi_{\vec{r}}^2 \rangle \langle \chi_{\vec{r}}^2 \rangle}}. \tag{7.17}$$

The average is again defined as $\langle a_{\vec{r}} \rangle = \frac{1}{N} \sum_{\vec{r}} a_{\vec{r}}$. The obtained correlation coefficient values are normalized, $C \in [-1, 1]$.

The GL coupling constants considered in the free energy F_{GL} of Equation (7.16), with indices $i = x, y$ and $s = 1, 2$, can be assigned estimates by evaluating the cross-correlation coefficients of corresponding nematic and smectic fields, according to Equation (7.17). We focus on couplings linear in nematic from now on (see discussion in Section 7.4). The precise choices of fields for each coupling constant are shown in Table 7.1. The resulting correlation coefficients are shown in Table 7.2.

The statistical significance of the correlation coefficient C can be assessed by calculating the probability $P(C, N)$ that two independent (uncorrelated) fields defined on the field-of-view with N pixels have a value of the correlation coefficient equal to, or larger than C. The $P(C^2, N)$ follows the Beta distribution:

$$P(C, N) = B\left(\frac{1}{2}, \frac{N-2}{2}\right)^{-1} (C^2)^{-1/2} (1 - C^2)^{N/2-2},$$

Table 7.1: The pairs of nematic and smectic fields that are cross-correlated according to Equation (7.17) to obtain the estimate of a GL coupling constant.

C	$\phi_{\vec{r}}$	$\chi_{\vec{r}}$
$\alpha_{i,s}$	$\delta O_n(\vec{r})$	$\lvert\psi_s(\vec{r})\rvert^2 \nabla_i \varphi_s(\vec{r}) = \frac{i}{2}\left(\psi_s \nabla_i \psi_s^* - \psi_s^* \nabla_i \psi_s\right)(\vec{r})$
β_s	$\delta O_n(\vec{r})$	$\lvert\psi_s(\vec{r})\rvert^2 - \langle\lvert\psi_s\rvert^2\rangle$

Table 7.2: The correlation coefficient C in percents, for nematic—smectic GL coupling terms of Eq. (7.16). The "high statistical significance" cutoff for $|C|$ is 13%.

%	$\alpha_{x,1}$	$\alpha_{x,2}$	$\alpha_{y,1}$	$\alpha_{y,2}$	β_1	β_2
C	-3	-10	1	16	18	2

with B the Beta function [254]. A criterion of significance can be then stated for C: If, for a given N and C of our datasets, there is more than 5% probability that completely independent datasets exhibit the same or higher correlation than C, i.e. $P(C, N) > 5\%$, then the found correlation is not statistically significant. The C in that case should be regarded as zero. In case of our datasets, this criterion says that cross-correlations having $|C| \geq 13\%$ are statistically significant. Our datasets are smoothed with a coarse-graining radius of Γ pixels (see SOM(I)). This means that the number of independent datapoints in the field-of-view is the number of pixels divided by the characteristic area under the Gaussian of width Γ used to smooth the fields. We therefore replace N by $N^{\text{eff}} \equiv N/(\Gamma^2\pi)$.

The statistical significance of the above cross-correlations in our data corroborates the use of GL theory.

7.4 Prediction of nematic fluctuations caused by stripe dislocations

In this Section we identify the signature of the coupling between the two OPs, and find it successfully compares with the experimental data. We need to consider the GL free energy $F_n[\delta O_n]$ for the nematic fluctuation (which is a real scalar field), taking the form of GL theory for an Ising field. This nematic GL free energy and the coupling terms in Equation (7.16) are used to predict the nematic fluctuation $\delta O_n^{(0)}(\vec{r})$ in the vicinity of a smectic dislocation shown in Figure 7.3. For this end we treat $F_n[\delta O_n]$ in the mean-field approximation, to arrive at the form (up to

an overall factor):

$$F_{MF}[\delta O_n, \psi_s] = \int \mathrm{d}^2\vec{r} \left[\sum_{i=x,y} (\nabla_i \delta O_n)^2 + \frac{1}{\xi_N^2} \delta O_n^2 + \delta O_n \sum_{s=1,2} |\psi_s|^2 \left\{ \sum_{i=x,y} \alpha_{i,s} \nabla_i \varphi_s + \beta_s \right\} \right], \tag{7.18}$$

where ξ_N is the nematic fluctuation correlation length, and for simplicity we have made the nematic fluctuation isotropic. The smectic field in the coupling term of Eq. (7.18) we regard as a source for the nematic fluctuation. The presence of coupling terms linear in nematic field then justifies the neglect of coupling quadratic in nematic, i.e. γ_s in Equation (7.16), which is therefore absent in Equation (7.18). More precisely, this term represents a weakly position dependent rescaling of the correlation length ξ_N and leads to minor quantitative effects. (The rescaling in question is $\xi_N \to \tilde{\xi}_N(\vec{r}) = [1 + \xi_N^2 \gamma_s |\psi_s|^2]^{-1/2} \xi_N$.)

To describe a single smectic dislocation we use the simplest model of a phase winding with smectic amplitude damped isotropically around the core:

$$|\psi_s(\vec{r})|^2 \nabla_i \varphi_s(\vec{r}) \equiv \left(1 - \exp\left(-|\vec{r}|^2/\xi_S^2\right)\right) \nabla_i \varphi_s^0(\vec{r}), \tag{7.19}$$

with $\varphi_s^0(\vec{r}) = \pm\theta$, where θ is the polar angle in the plane (see Fig. 7.3 and Eq. (7.10)); here the smectic dislocation has phase winding equal to $\pm 2\pi$. The ξ_S is the coherence length of the smectic. An example of this smectic field profile, which acts as a source for nematic fluctuation, is shown in Figure 7.3. From Fig. 7.3 it is obvious that the characteristic smectic phase profile $\varphi_s^0(\vec{r})$ of a dislocation is responsible for the robust features of the smectic source field, in particular a dipole field profile with a domain boundary at the dislocation. These features are directly transferred to the nematic fluctuation $\delta O_n^{(0)}(\vec{r})$, and are observed in the experimental data (Figure 7.4(a)). The linear coupling of nematic to the smectic amplitude (β_s in Equation (7.16)) provides an overall shift of the source field, and therefore does not influence these robust features, unless $\beta_s \gg \alpha_{i,s}$.

The key, robust prediction of the coupling is that $\delta O_n^{(0)}(\vec{r})$ will vanish on a line passing through the core of a smectic dislocation. This can be qualitatively understood from the analogy between our free energy F_{GL} (or F_{MF}), the Eq. (7.14), and a flux line in a type-II superconductor. For the analogy, let us consider only the covariant derivative coupling term in the free energy for one of the smectic modulations, say $s = 1$ in Eq. (7.16), with $a_{x,1} = a_{y,1}$ for simplicity. In a superconductor, the integer winding of the superconducting phase in a vortex is precisely canceled by a vortex profile of the electromagnetic potential, i.e. the appearance of a quantized magnetic flux tube, thereby leading to the vanishing of such a free energy. In our case, the winding in the smectic phase cannot be entirely canceled by the nematic term, because the nematic term is directed along a constant vector $\vec{c}$ (assumed of unit length). There is no quantization in the nematic field. Instead, to minimize the free energy, the two fields cancel only

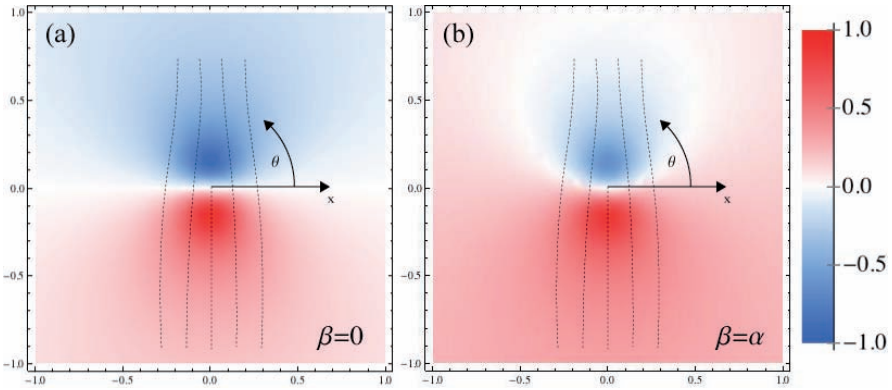

Figure 7.3: (a) Source field from a stripe ψ_1 dislocation, according to Equation (7.19). This source field, $|\psi_1(\vec{r})|^2\nabla_x\varphi_1(\vec{r})$, is weighed by the coupling constant $\alpha_{1,1}$, and we fix $\beta_s \equiv 0$. Dashed lines schematically represent the peaks of the stripe density wave. The characteristic dipole shaped pattern, with its domain boundary on the x-axis, is robustly transferred from this source field onto the nematic fluctuation. (b) The source field when stripe amplitude—nematic fluctuation coupling is switched on, for the example value $\beta_1 = \alpha_{1,1}$. This amplitude coupling β_s only provides an overall shift of the pattern and does not influence the robust features, as long as β is not much greater than α.

along the vector $\vec{c}$, giving

$$\delta O_n^{(0)}(\vec{r}) = \vec{c}\cdot\vec{\nabla}\,\varphi_1^0(\vec{r}) \tag{7.20}$$

Since the smectic phase $\varphi_1^0(\vec{r})$ is in the form of a vortex, the field $\delta O_n^{(0)}(\vec{r})$ vanishes along the direction of the vector $\vec{c}$, as announced.

To find the nematic fluctuation $\delta O_n^{(0)}(\vec{r})$ quantitatively, we use the Green's function of δO_n in $F_{MF}[\delta O_n, \psi_s]$, with the smectic dislocation acting as the source of the form given in Equation (7.19). The Green's function takes the homogeneous and isotropic form $G(\vec{r}) = K_0(|\vec{r}|/\xi_N)$, with $K(r)$ the Bessel function of the second kind. The resulting response of the nematic fluctuation field

$$\delta O_n^{(0)}(\vec{r}) = \int \mathrm{d}^2\vec{r}'\, G(\vec{r}-\vec{r}') \sum_{s=1,2} |\psi_s(\vec{r}')|^2 \left\{ \sum_{i=x,y} \alpha_{i,s}\nabla_i\varphi_s(\vec{r}') + \beta_s \right\} \tag{7.21}$$

is shown in Figure 7.3 for the particular example of ψ_1 dislocation (i.e. $s = 1$ is fixed) and the choice $(\alpha_{x,1}, \alpha_{y,1}) = (1, 0)$. The characteristic features inherited from the smectic source field of Figure 7.3 are: (i) The nematic fluctuation boundary direction is aligned with the smectic modulation wavevector $\vec{S}_x$, and (ii) the locations of high positive (high negative) nematic fluctuation corresponds to the

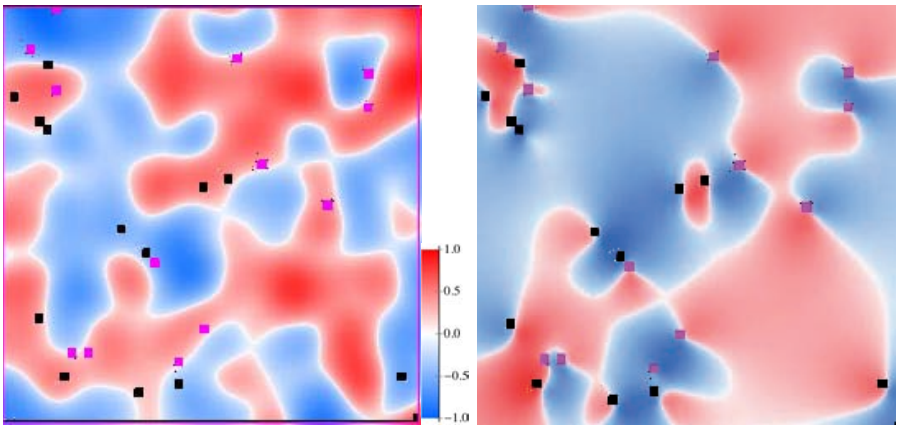

(a) Dots mark the stripe dislocations superimposed on the nematic field fluctuations $\delta O_n = O_n - \langle O_n \rangle$.

(b) The simulation of nematic fluctuation $\delta O_n^{(0)}(\vec{r})$, according to Eq. (7.21), with $L/\xi_N = 36$.

Figure 7.4: The nematic fluctuation in relation to stripe dislocations

area on the side of the smectic dislocation where the smectic is locally stretched (compressed). Rotating the coupling constants away from chosen value causes a rotation of the smectic source field, and the resulting nematic fluctuation pattern.

To actually compare the prediction with experimental data, we start by replacing the smectic fields by a superposition of single dislocation fields, with dislocation locations and windings determined from the experimental datasets. We check that the resulting smectic fields are almost identical to the experimental ones, meaning that it is a reasonable assumption that the dislocations determine the fluctuation of smectic fields. We then find the simulated $\delta O_n^{(0)}(\vec{r})$ field (shown in Figure 7.4(b)) using Eq. (7.21), which is compared to the experimental data shown in Figure 7.4(a). We set $\xi_S/\xi_N = 0.1$ in the figures, based on the fact that the experimental data shows larger correlation lengths for the nematic than the smectic fluctuations. It is also possible to find the values of the phenomenological coupling constants (assuming they do not vary spatially) $\alpha_{i,s} \equiv (\alpha_{x,1}, \alpha_{x,2}, \alpha_{y,1}, \alpha_{y,2}) = (-1, 0.7, 0, 1)$ such that the simulated $\delta O_n^{(0)}(\vec{r})$ field fits the experimentally observed one. The resulting agreement of the data and the simulation, shown in Fig. 7.4, is quite satisfactory visually, while the correlation coefficient is $C = 15\%$, which rates as highly significant. The ratios and signs of GL coupling constants estimated in this way roughly match the guiding values obtained by the cross-correlation procedure presented in the previous Section.

7.5 Discussion and concluding remarks

The direct observation of stripe dislocations, and exponential decay of stripe correlations, indicate that the viewpoint of underdoped cuprates as a phase of fluctuating quantum smectic which melts through defects [35, 100–102] is indeed of direct relevance. Within this interpretation, the question becomes what is the expected relation to the nematic order? One expects that a $\vec{S}_a$ stripe represents a smectic phase in which the original (bosonized) electronic crystal has melted through a condensation of crystal dislocations with Burgers vectors $\vec{b} \perp \vec{e}_a$ (let us call these the "original" dislocations). Incommensuration signifies a floating solid of original electrons [34]. Appearance of stripe dislocations is then further restoring all translational symmetry and leaving only an orientational order — the dislocations should therefore correlate with strong orientational order, called a "nematic". However, this nematic order just means that isotropic rotations are broken to a subgroup: if the stripe dislocations contribute the same as the "original" dislocations, the result is a C_{4v} state — and this is indistinguishable from the original lattice symmetry! In the somewhat analogous classical situation [34], melting of a floating triangular lattice by dislocations into the orientationally ordered "hexatic" can even be completely absent, and isotropic fluid is directly obtained. If we accept that an identified single $\vec{S}_a$ stripe dislocation at position $\vec{r}$ contributes less to the symmetry restoration than the condensate of "original" dislocations constituting the stripe, we must conclude that around point $\vec{r}$ the created nematic state will have a C_{2v} symmetry, and be oriented perpendicularly to $\vec{S}_a$. One should therefore be careful in discussing the relation of stripes and a "nematic" order.

Concerning the definition of "nematic" we have found relevant in the data, it is a crystal Bragg peak order, having the translational symmetry of the lattice, and a C_{2v} orientational symmetry. It is therefore an intra-unit-cell order, resembling an orthorombicity order parameter. In view of the preceding paragraph, the fact that we do not observe a direct correlation between stripe dislocations and the strength of our nematic order parameter, might mean that stripes melt into the "tetratic" (analogue of "hexatic") type of nematic; this should properly be identified as the "isotropic nematic" of Ref. [35]. The argument against the "topological nematic" is that the stripe dislocations and the "original" dislocations are two separate condensates, contributing equally. One should be aware that ongoing research might show that the naively expected direct correlation exists, but it is weak.

The stripes still interact strongly with the *fluctuation* of the intra-unit-cell nematic, as we uncovered in this Chapter. This might be a direct consequence of the weak correlation of melted stripes and the C_{2v} version of the nematic, a theme that should certainly be further investigated.

A final point focusing on stripe melting is that both stripe directions seem suppressed at sites of single stripe dislocations, Fig. 7.2. This might represent the fact that a stripe dislocation signifies a local complete restoration of translational

symmetry, and therefore in the same spatial area we do not expect strong presence of the other stripe (which would be again translational symmetry breaking).

The type of independent behavior of intra-unit-cell nematic that we found is also indicative of its "microscopic" nature. Namely, the situation suggests that the intra-unit-cell order, in form of oriented Cu—O—Cu "bars", might represent the singlet pairs taking the role of Cooper pairs, which are the active elements of resonating valence bond (RVB) type theories of superconductivity, e.g. Refs. [92,255]. The present study shows that these "valence bond" bars show ordering, but, unexpectedly, the stripes are not straightforwardly formed from a simple stacking of these building blocks. In other words, the nematic order is directly descending from the valence bonds, but the translational order depins from the lattice dominated by microscopic building blocks.

Finally, let us mention that preliminary analysis hints at a connection between dislocation positions and the position of dopants which represent external disorder. Because of this possibility, it is important to note that the coupling mechanism presented here provides a way for impurities to act as a "random mass" parameter, as opposed to the commonly believed case of a "random field" parameter, on the Ising-like nematic OP [256].